IL NUOVO CIMENTO **44 C** (2021) 175
DOI 10.1393/ncc/i2021-21175-5

COLLOQUIA: La Thuile 2021

Recent results from Belle II

E. TORASSA(*)
INFN, Sezione di Padova - Padova, Italy

received 16 September 2021

Summary. — Belle II is a major upgrade of the previous Belle experiment. The Belle II detector has been installed in the interaction region of the SuperKEKB e^+e^- collider located at the KEK laboratory in Tsukuba. The beam-beam collisions started in March 2018 and the integrated luminosity of data collected up to March 2021 was about 100 fb^{-1}. The target of the experiment is to collect 50 ab^{-1} of data within 2031 by means of a progressive increase of the instantaneous luminosity up to the target of 6×10^{35} $\text{cm}^{-2}\text{s}^{-1}$. In these proceedings recent results of the Belle II experiment are reported using a fraction of collected data, which is between 280 pb^{-1} and 35 fb^{-1} of integrated luminosity depending to the physics analysis.

1. – Introduction

During the first decade of this century the BaBar and Belle experiments collected together about 1.5 ab^{-1} of integrated luminosity and recorded about 1.2 billions of B meson pairs, with which they performed precise measurements of the Cabibbo-Kobayashi-Maskawa (CKM) matrix parameters. Several measurements of B meson decays performed in the last years by the BaBar, Belle and LHCb experiments reported deviations of about 3σ from the Standard Mode (SM) expectations [1]. The recent measurement of the Muon g-2 collaboration about the muon anomalous magnetic moment [2] confirmed a deviation of about 4σ from the SM expectation. SuperKEKB and Belle II can further improve significantly the precision of the CKM matrix parameters and will help to clarify whether or not these anomalies are due to contributions of new physics that are comparable with the SM amplitudes.

2. – SuperKEKB and Belle II

The SuperKEKB collider [3] consists of two storage rings. In the high energy ring electrons are accelerated to the energy of 7.0 GeV, in the low energy ring positrons are accelerated to the energy of 4.0 GeV. The center-of-mass (CMS) energy of 10.58 GeV

(*) On behalf of the Belle II Collaboration.

is the peak of the $\Upsilon(4S)$ production cross section. The $\Upsilon(4S)$ off-resonance energy scan and the study of other bottomonium resonances are part of the physics program. Using the "nano beam" technique [4] SuperKEKB shrinks the vertical beam size to tens of nanometers at the collision point. The upgrade of the colliding scheme with respect to the KEKB collider will provide an increase of the maximum instantaneous luminosity by a factor 30 and of the total integrated luminosity by a factor 50. The Belle II detector consists of several subsystems. The tracking system is composed of the pixel vertex detector, the silicon strip vertex detector and the central drift chamber (CDC). Outside the CDC, a Cherenkov-light detector with time-of-propagation measurement provides charged-particle identification in the barrel region. An aerogel ring imaging Cherenkov detector is located in the forward region. Further out an electromagnetic calorimeter (ECL), consisting of a barrel and two endcap sections provides photon and electron identification and energy reconstruction. A superconducting solenoid situated outside the calorimeter produces a uniform 1.5 T magnetic field. Multiple layers of scintillators and resistive plate chambers, located between the magnetic flux-return iron plates, constitute the K_L and muon identification system. Similar subsystems were already present in the Belle detector but the new subsystems have better performance, the electronics have been upgraded and a new trigger for low multiplicity and dark sector searches has been introduced.

3. – Detector performance

The particle identification performance has been tested by measuring the charged kaon and pion separation using the $D^{*+} \to D^0(K^-\pi^+)\pi_s^+$ decay [5]. The charge conjugated mode is also included. The charge of the slow pion π_s^+ can be used to derive the flavor of the D^0, which is used to identify the K^- and the π^+. With the likelihood ratio selection $\mathcal{L}_K/(\mathcal{L}_K + \mathcal{L}_\pi) > 0.5$, the measured kaon efficiency and pion misidentification rate are close to the values expected from the Monte Carlo simulation with a maximum discrepancy of about 5% (fig. 1 left). The tracking efficiency has been measured using $e^+e^- \to \tau^+\tau^-$ events, where one tau lepton decays leptonically ($\tau^\pm \to \ell^\pm\nu_\ell\bar{\nu}_\tau$) while the other decays hadronically into three charged pions ($\tau^\pm \to 3\pi^\pm\nu_\tau + n\pi^0$) [6]. Three charged tracks ($\ell^\pm\pi^\mp\pi^\mp$) tag the $\tau^+\tau^-$ events and we measure the efficiency of reconstructing the fourth track as a function of its transverse momentum (fig. 1 right).

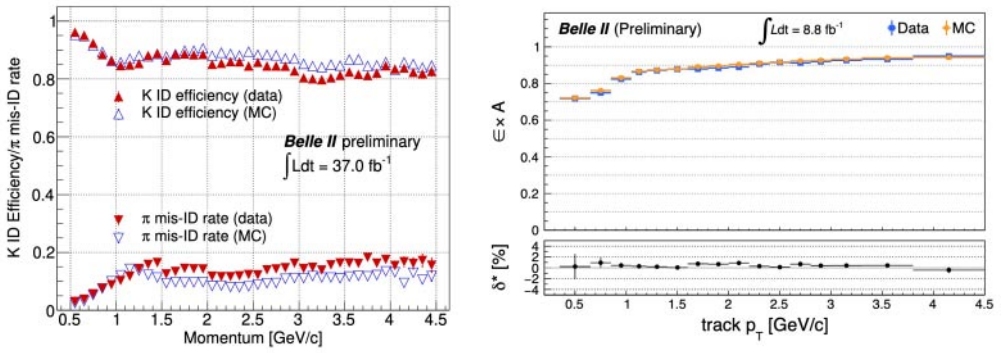

Fig. 1. – Kaon efficiency and pion misidentification rate as a function of the momentum (left). Tracking efficiency times detector acceptance as a function of the transverse momentum (right).

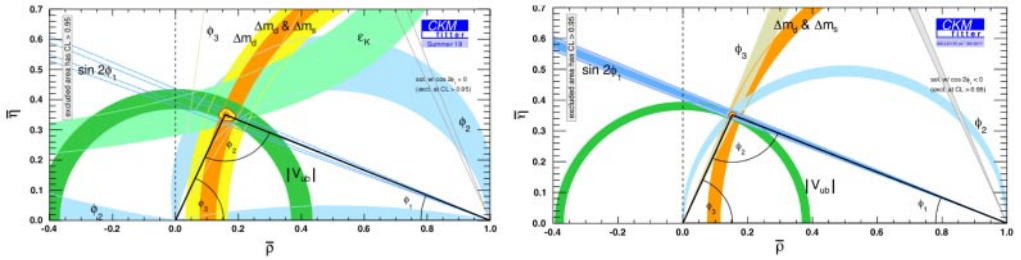

Fig. 2. – The CKM unitarity triangle fitted by the CKMfitter group in Summer 2019 (left). The CKM unitarity triangle extrapolated to the Belle II integrated luminosity of 50 ab^{-1} and LHCb integrated luminosity of 22 fb^{-1} (right) for a SM-like scenario.

4. – Physics prospects

The Belle II experiment is covering several physics topics: leptonic and semi-leptonic B decays, radiative and electroweak penguin B decays, time dependent CP violation in B decays, hadronic B decays, charm physics, τ lepton and low multiplicity physics, quarkonium, dark sector and beyond the Standard Model. The details of the physics prospects can be found in "The Belle II Physics Book" [7]. Figure 2 shows the CKM unitary triangle global fit for the Wolfenstein parameters $\bar{\eta}, \bar{\rho}$ performed by the CKMfitter group in 2019 [8] and the extrapolation to the Belle II integrated luminosity of 50 ab^{-1} and LHCb integrated luminosity of 22 fb^{-1} with the assumption of a significant improvement in lattice QCD calculations for B semileptonic decays and $B^0 - \bar{B}^0$ mixing for a SM-like scenario [7]. The errors on the CKM angles are expected to be reduced for ϕ_1 from $\pm 1^o$ to $\pm 0.3^o$, for ϕ_2 from $\pm 3.2^o$ to $\pm 0.6^o$, for ϕ_3 from $\pm 3.0^o$ to $\pm 0.6^o$.

5. – Search for an invisibly decaying Z' boson

In the $U(1)_{L_\mu - L_\tau}$ gauge symmetry extension of the SM, the spontaneous symmetry breaking gives rise to a neutral boson Z' couplings only with μ, ν_μ, τ and ν_τ leptons with coupling constant g'. The $L_\mu - L_\tau$ model is potentially able to address important open issues in particle physics, including the anomaly in the muon anomalous magnetic moment $(g-2)_\mu$ [2]. The Z' boson can have invisible decays to neutrinos or to new dark particles [9]. We consider also an alternative model, which introduces lepton-flavor violating (LFV) mediator boson with spin 0 or 1 [10] [11]. In this model the new mediator is coupling with the SM fermions with a coupling constant g' only through flavor violating interactions. The data used in this analysis [12] were collected from April to July 2018 at the CMS energy of the $\Upsilon(4S)$ resonance. The integrated luminosity, after data quality requirements on particle identification have been applied, amounts to 276 pb^{-1}. The search for an invisibly decaying Z' boson is performed by requiring two opposite charged leptons ($\mu^\pm\mu^\mp$ or $e^\pm\mu^\mp$). The signal signature should be a bump in the distribution of the recoil mass. The final recoil mass spectrum of the $\mu^+\mu^-$ and $e^\pm\mu^\mp$ samples are shown in fig. 3, together with the expected backgrounds. No anomalies have been observed above 3σ local significance. Figure 4 (left) shows the upper limits (UL) on the Z' cross section at 90% confidence level (C.L.) as a function of the coupling constant g' and $M_{Z'}$ for the $L_\mu - L_\tau$ model. The dark blue and light blue filled areas show the exclusion regions assuming the $L_\mu - L_\tau$ predicted branching ratio ($\mathcal{B}$) for $Z' \to$ invisible

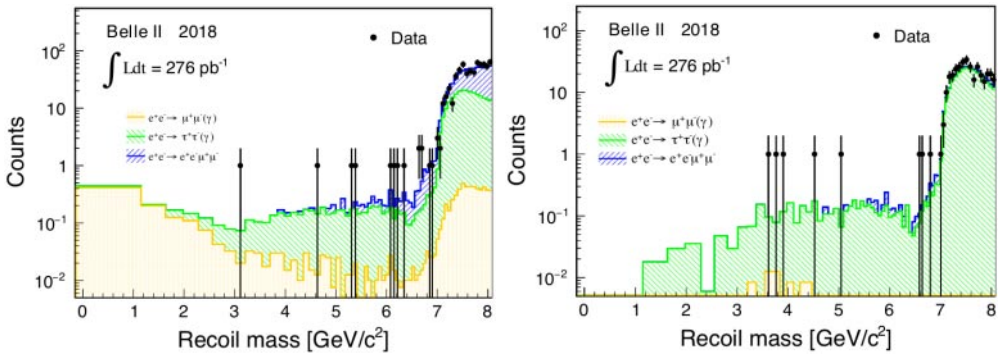

Fig. 3. – Recoil mass spectrum of the $\mu^+\mu^-$ sample (left) and of the $e^\pm\mu^\mp$ sample (right) together with the simulated SM backgrounds.

and the $\mathcal{B}(Z' \to \text{invisible}) = 1$ respectively. The red band shows the region that could explain the muon anomalous magnetic moment within 2σ. Figure 4 (right) shows the model-independent UL on the efficiency times cross section as a function of the recoil mass for the LFV $Z' \to$ invisible decay.

6. – Search for axionlike particles

Axions and axionlike particles (ALPs) are singlet neutral scalar or pseudoscalar predicted by many extensions of the Standard Model [13]. We consider the case where the ALP predominantly couples to photons so $\mathcal{B}(\text{a} \to \gamma\gamma) \approx 100\%$. The data used in this analysis [14] were collected from April to July 2018 at the CMS energy of the $\Upsilon(4S)$ resonance. The integrated luminosity amounts to 496 pb^{-1}. About 10% of data was used for the selection validation and discarded from the data sample. The residual integrated luminosity amounts to 445 pb^{-1}. When selecting events with three photons in the final state, the signal is identified by a narrow peak in the 2γ invariant mass or a narrow

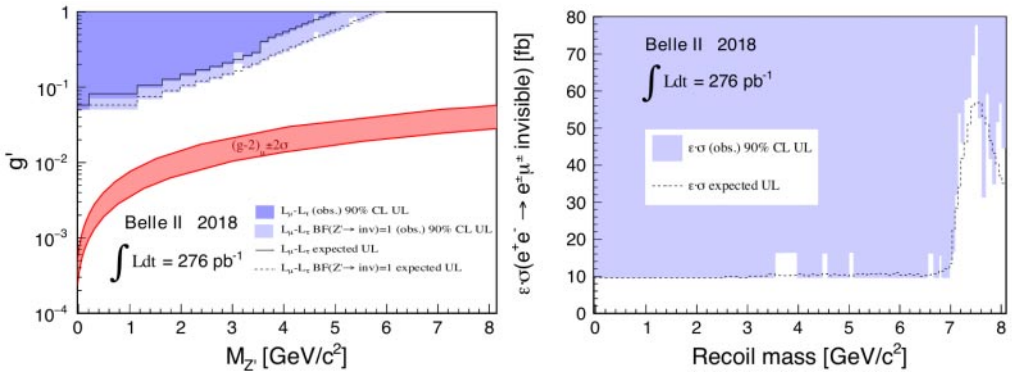

Fig. 4. – Upper limits on the Z' cross section at 90% C.L. as a function of the coupling constant g' and $M_{Z'}$ for the $L_\mu - L_\tau$ model (left). Model-independent upper limits on the LFV Z' efficiency times cross section at 90% C.L. as a function of the recoil mass (right).

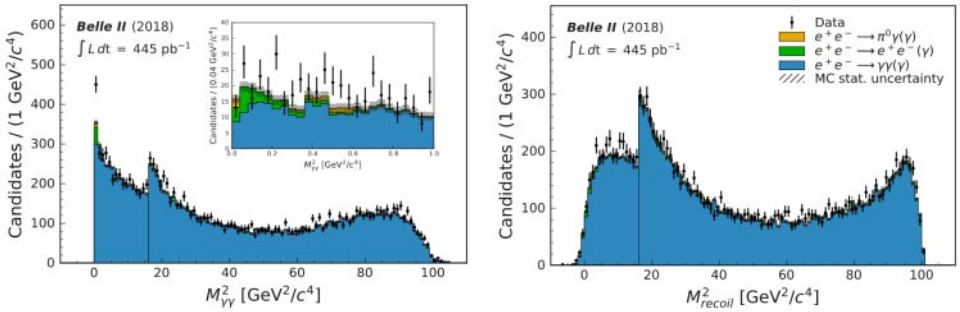

Fig. 5. – $M^2_{\gamma\gamma}$ (left) and M^2_{recoil} (right) distributions together with the simulated backgrounds.

peak in the squared recoil mass distribution $M^2_{\mathrm{recoil}} = s - 2\sqrt{s}E^{\mathrm{CMS}}_{\mathrm{recoil}(\gamma)}$ were recoil(γ) is the most energetic photon recoiling against the other two. The expected resolution on the ALP mass m_{a} has been estimated with a simulated signal sample and it turns out to be better for the di-photon method for $m_{\mathrm{a}} < 6.5$ GeV/c^2 and for the recoil method for $m_{\mathrm{a}} > 6.5$ GeV/c^2. The resulting $M^2_{\gamma\gamma}$ and M^2_{recoil} distributions are shown in fig. 5. We find no evidence for ALPs and set 95% C.L. upper limits on the ALP cross section σ_{a} (fig. 6, left). The 95% C.L. upper limit on the ALP-photon coupling as a function of the ALP mass is shown in fig. 6 (right). The exclusion region outlined by previous experiments has been extended already with ~ 0.5 fb^{-1}.

7. – Measurement of the semileptonic $\overline{B}^0 \to D^{*+}\ell^-\overline{\nu}_l$ branching fraction

Precision measurements of the branching ratio for the $\overline{B}^0 \to D^{*+}\ell^-\overline{\nu}_l$ decay play an important role in the determination of the CKM matrix element $|V_{cb}|$. We measured the branching ratio for the muon and electron decays using two different methods of B meson reconstruction: the full event interpretation (FEI) [15] and the untagged method [16]. With FEI one of the B mesons (B_{tag}) of the $B^0 - \bar{B}^0$ pair is reconstructed from a large set of hadronic decays and is used to extract the signal from the other B meson having a semileptonic decay. The untagged method consists in constraining the direction of the

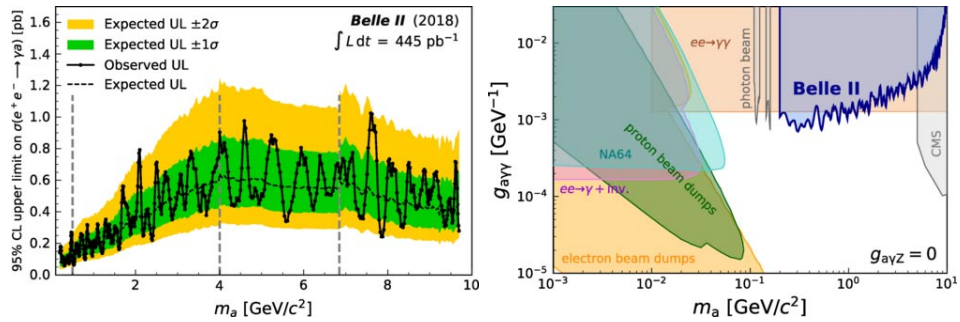

Fig. 6. – Expected and observed 95% C.L. upper limits on the ALP cross section σ_{a} (left). The 95% C.L. upper limit on the ALP-photon coupling as a function of the ALP mass from this analysis and previous experiments (right).

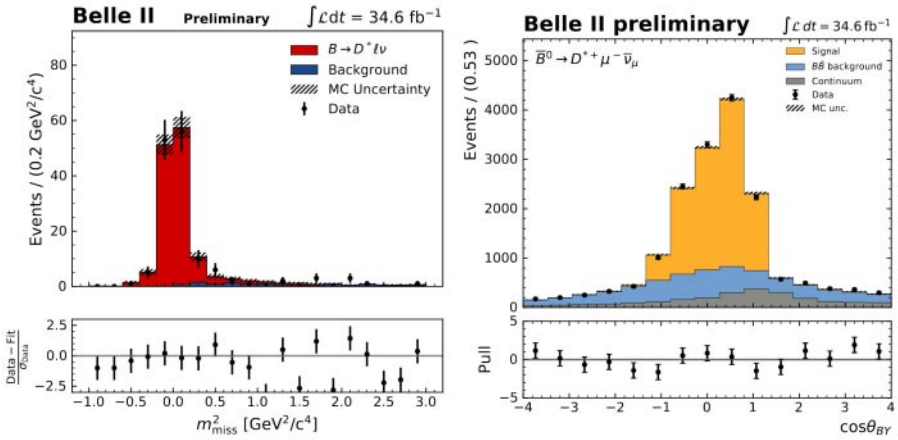

Fig. 7. – $m^2_{\rm miss}$ distribution for the FEI $\overline{B}^0 \to D^{*+}\ell^-\overline{\nu}_l$ candidates (left). The fitted $\cos\theta_{BY}$ distribution for the selected untagged $\overline{B}^0 \to D^{*+}\mu^-\overline{\nu}_l$ candidates (right) with SM backgrounds.

momentum of the B meson to lie on a cone around the direction of the $D^{*+}\ell^-$ system (denoted as Y). The modulus of the B meson's momentum in the CMS frame of the collision can be determined using the nominal B mass and the energy of the collision. D^{*+} are reconstructed from the decay cascade $D^{*+} \to D^0\pi_s^+$ and $D^0 \to K^-\pi^+$. The data used in these two analyses have been collected from March 2019 to May 2020 corresponding to an integrated luminosity of 34.6 fb^{-1}. Figure 7 (left) shows the missing mass distribution $m^2_{\rm miss}$ [15] for events containing the reconstructed B meson; this distribution should peak close to $m^2_{\rm miss} \sim m^2_\nu \sim 0$. Figure 7 (right) shows the angle between Y and the B meson direction in the CMS frame of the collision. Corrections for hadrons misidentified as leptons are obtained from samples of reconstructed $K_S \to \pi^+\pi^-$ decays. The measured branching fractions are:

$$\mathcal{B}^{\rm FEI}(\overline{B}^0 \to D^{*+}\ell^-\overline{\nu}_l) = (4.51 \pm 0.41_{\rm stat} \pm 0.27_{\rm syst} \pm 0.45_{\pi_s})\%;$$
$$\mathcal{B}^{\rm Untag}(\overline{B}^0 \to D^{*+}\ell^-\overline{\nu}_l) = (4.60 \pm 0.05_{\rm stat} \pm 0.17_{\rm syst} \pm 0.45_{\pi_s})\%.$$

The dominant systematic uncertainty π_s, derives from the uncertainty on the low momentum tracking efficiency, which is currently limited by the low statistics. A test of the LFV is performed with the ratio of the electron and muon branching fraction ($R_{e\mu}$) using the more precise untagged measurements. The $\mathcal{B}^{\rm FEI}$, $\mathcal{B}^{\rm Untag}$ and $R_{e\mu} = 0.99 \pm 0.03$ measurements are compatible with the SM expectations.

8. – $B^0 - \bar{B}^0$ mixing and time-dependent CPV

One of the major goals of the Belle II physics program is to improve the measurement of the CKM matrix parameters. The $B^0 - \bar{B}^0$ oscillation was measured with the hadronic $B^0 \to D^-(K^+\pi^-\pi^-)\pi^+$ decay. The charge of the D meson tags the flavor of the B meson [17]. B meson pairs, produced with opposite flavor from $\Upsilon(4S)$, can oscillate producing mixed or unmixed decays. The mixing asymmetry is computed as a function of the difference between the two B meson decay times (Δt) because $A_{\rm mixing}(\Delta t) = \frac{N^{\rm unmixed} - N^{\rm mixed}}{N^{\rm unmixed} + N^{\rm mixed}} = D\ \cos(\Delta m_d\ \Delta t)$ where $D = (1 - 2w)$ and w is the wrong tag fraction.

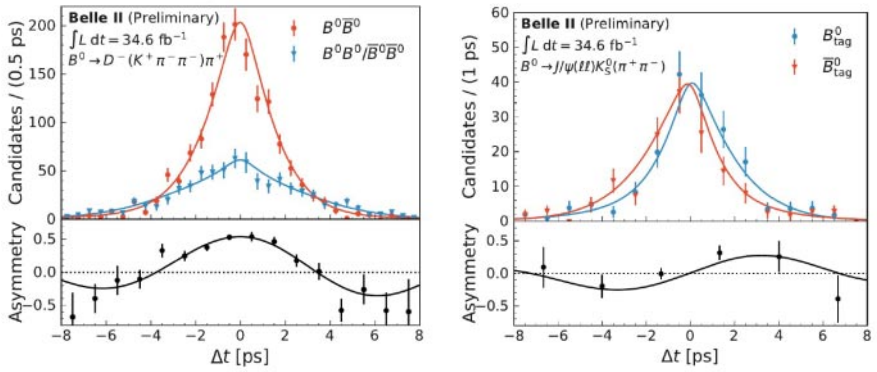

Fig. 8. – Δt distribution and asymmetry for same flavor and opposite flavor B mesons reconstructed in the hadronic $B^0 \to D^-(K^+\pi^-\pi^-)\pi^+$ decay (left). Δt distribution and asymmetry for the $B^0_{\rm tag}$ and $\bar{B}^0_{\rm tag}$ reconstructed in the "golden" $B^0 \to J/\Psi K_S$ decay (right).

The time-dependent CPV was measured with the "golden" channel $B^0 \to J/\Psi K_S$. The B^0 or $\bar{B}^0$ flavor is determined using the information from the decay products of the opposite side B meson. The tag asymmetry as a function of Δt is related to the angle ϕ_1 of the CKM matrix: $A_{\rm CP}(\Delta t) = \frac{N(\bar{B}^0 \to J/\Psi K_S) - N(B^0 \to J/\Psi K_S)}{N(\bar{B}^0 \to J/\Psi K_S) + N(B^0 \to J/\Psi K_S)} = D \sin(2\phi_1) \sin(\Delta m_d\ \Delta t)$. The data used in these two analysis have been collected from March 2019 to May 2020 corresponding to an integrated luminosity of 34.6 fb^{-1} [18]. Figure 8 (left) shows the Δt distribution for reconstructed $B^0 \to D^-(K^+\pi^-\pi^-)\pi^+$ candidates. Figure 8 (right) shows the Δt distribution for reconstructed $B^0 \to J/\Psi K_S$ candidates. The measured $\Delta\ m_d = (0.531 \pm 0.046_{\rm stat} \pm 0.013_{\rm syst})$ ps^{-1} and $\sin(2\phi_1) = 0.55 \pm 0.21_{\rm stat} \pm 0.04_{\rm syst}$ are compatible with the world average $\Delta m_d = (0.5065 \pm 0.0019)$ ps^{-1} and $\sin(2\phi_1) = 0.699 \pm 0.0017$ [1].

9. – τ mass measurement

The τ mass measurement uses data corresponding to an integrated luminosity of 8.8 fb^{-1} accumulated during 2019 at $\sqrt{s} = 10.58$ GeV [19]. In the $e^+e^- \to \tau^+\tau^-$ centre-of-mass system, both τ leptons are back-to-back and their decay products are well separated in two opposite hemispheres. One hemisphere is expected to contain the products of three-prong τ decay ($\tau^+ \to \pi^+\pi^-\pi^+\bar{\nu}_\tau$), while the other one the products of one-prong τ decay ($\tau^- \to \ell^-\bar{\nu}_\ell\nu_\tau$ or $\tau^- \to h^-\nu_\tau$ or $\tau^- \to \pi^-\pi^0\nu_\tau$). The identification of charged particles is based on the ratio between the energy deposit in the ECL and the momentum of the particle measured by the tracking system: $E_{\rm ECL}/P_{\rm lab} < 0.8$. The pseudo mass is defined as $M_{\rm min} = \sqrt{M^2_{3\pi} + 2(E_{\rm beam} - E_{3\pi})(E_{3\pi} - P_{3\pi})}$ where $E_{\rm beam}$ is the beam energy, and $M_{3\pi}$, $E_{3\pi}$, $P_{3\pi}$ stand for the invariant mass, energy and momentum, respectively, of the three pion system in the CMS. In the absence of initial and final state radiation, and with a perfect measurement of the four-momentum of the hadronic system, the $M_{\rm min}$ distribution has a sharp edge at m_τ. The τ mass is measured with a best fit in a range of $M_{\rm min}$ between 1.7 GeV and 1.85 GeV (fig. 9 left). The measurement of $m_\tau = 1777.28 \pm 0.75$ (stat.) ± 0.33 (syst.) MeV/c^2 is in good agreement with the current world average (fig. 9 right). The Belle II τ mass measurement is expected to be statistically dominated until around 50 fb^{-1} of data.

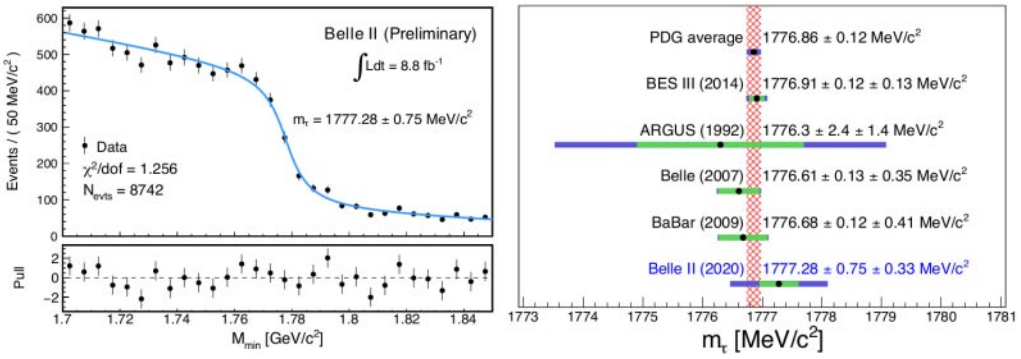

Fig. 9. – The pseudomass ($M_{\min}$) distribution in the data sample and the results of the fit (left). The τ mass measurement of Belle II compared to various experiments and to the PDG average. The green and blue bands indicate the systematic and total uncertainties, respectively (right).

10. – Conclusions

The SuperKEKB e^+e^- collider started beam-beam collisions in March 2018. The integrated luminosity of data collected by early March 2021 was about 100 fb^{-1}. The data collected in the 2018 commissioning run resulted in two Physical Review Letter publications on Z' and axion-like searches adding new exclusion limits in the dark sector. Some analyses have been reported here and several others are ongoing. We plan to accumulate similar statistics with respect to the BaBar and Belle experiments by 2022 hence becoming competitive with them in all the analyses.

REFERENCES

[1] HFLAV (Amhis Y. *et al.*), *Eur. Phys. J. C*, **81** (2021) 226.
[2] Muon g-2 Collaboration (Abi B. *et al.*), *Phys. Rev. Lett.*, **126** (2021) 141801.
[3] SuperKEKB Accelerator Team (Akari K. *et al.*), *Nucl. Instrum. Methods Phys. Res. A*, **907** (2018) 188.
[4] SuperB Collaboration (Baszczyk M. *et al.*), arXiv:1306.5655 [physics.ins-det].
[5] The Belle II Collaboration, BELLE2-NOTE-PL-2020-024.
[6] The Belle II Collaboration, BELLE2-NOTE-PL-2020-014.
[7] Belle II Collaboration (Kou E. *et al.*), *Prog. Theor. Exp. Phys.*, **2019** (2019) 123C01.
[8] CKMfitter Group Collaboration (Charles J. *et al.*), *Eur. Phys. J. C*, **41** (2005) 1, updated results and plots available at `http://ckmfitter.in2p3.fr`.
[9] Curtin D., Essig R., Gori S., and Shelton J., *JHEP*, **02** (2015) 157.
[10] Galon I. and Zupan J., *JHEP*, **05** (2017) 083.
[11] Galon I., Kwa A., and Tanedo P., *JHEP*, **03** (2017) 064.
[12] Belle II Collaboration (Adachi I. *et al.*), *Phys. Rev. Lett.*, **124** (2020) 141801.
[13] Jaeckel J. and Ringwald A., *Annu. Rev. Nucl. Part. Sci.*, **60** (2010) 405.
[14] Belle II Collaboration (Abudinén F. *et al.*), *Phys. Rev. Lett.*, **125** (2020) 161806.
[15] Belle II Collaboration (Abudinén F. *et al.*), arXiv:2008.10299 [hep-ex].
[16] Belle II Collaboration (Abudinén F. *et al.*), arXiv:2008.07198 [hep-ex].
[17] Belle II Collaboration (Abudinén F. *et al.*), arXiv:2008.02707 [hep-ex].
[18] Belle II Collaboration (Abudinén F. *et al.*), BELLE2-NOTE-PL-2020-011.
[19] Belle II Collaboration (Abudinén F. *et al.*), arXiv:2008.04665 [hep-ex].